Molecular crowders and cosolutes promote folding cooperativity of RNA under physiological ionic conditions

CHRISTOPHER A. STRULSON,[1,2] JOSHUA A. BOYER,[1,2] ELISABETH E. WHITMAN,[1,2] and PHILIP C. BEVILACQUA[1,2,3]

[1]Department of Chemistry, The Pennsylvania State University, University Park, Pennsylvania 16802, USA
[2]Center for RNA Molecular Biology, The Pennsylvania State University, University Park, Pennsylvania 16802, USA

ABSTRACT

Folding mechanisms of functional RNAs under idealized in vitro conditions of dilute solution and high ionic strength have been well studied. Comparatively little is known, however, about mechanisms for folding of RNA in vivo where Mg^{2+} ion concentrations are low, K^+ concentrations are modest, and concentrations of macromolecular crowders and low-molecular-weight cosolutes are high. Herein, we apply a combination of biophysical and structure mapping techniques to tRNA to elucidate thermodynamic and functional principles that govern RNA folding under in vivo–like conditions. We show by thermal denaturation and SHAPE studies that tRNA folding cooperativity increases in physiologically low concentrations of Mg^{2+} (0.5–2 mM) and K^+ (140 mM) if the solution is supplemented with physiological amounts (~20%) of a water-soluble neutral macromolecular crowding agent such as PEG or dextran. Low-molecular-weight cosolutes show varying effects on tRNA folding cooperativity, increasing or decreasing it based on the identity of the cosolute. For those additives that increase folding cooperativity, the gain is manifested in sharpened two-state-like folding transitions for full-length tRNA over its secondary structural elements. Temperature-dependent SHAPE experiments in the absence and presence of crowders and cosolutes reveal extent of cooperative folding of tRNA on a nucleotide basis and are consistent with the melting studies. Mechanistically, crowding agents appear to promote cooperativity by stabilizing tertiary structure, while those low molecular cosolutes that promote cooperativity stabilize tertiary structure and/or destabilize secondary structure. Cooperative folding of functional RNA under physiological-like conditions parallels the behavior of many proteins and has implications for cellular RNA folding kinetics and evolution.

Keywords: folding cooperativity; tRNA; macromolecular crowding; biological cosolutes; temperature-dependent structure mapping

INTRODUCTION

The last decade has witnessed remarkable advances in understanding RNA folding from a physical–chemical perspective. Tertiary folding of complex RNAs begins with rapid electrostatic collapse, followed by search for the native state (Thirumalai et al. 2001; Russell et al. 2002; Moghaddam et al. 2009). This occurs on a rough landscape (Woodson 2010; Takamoto et al. 2012) wherein misfolds are broken prior to native folding (Thirumalai et al. 2001). These features can lead to very slow (minutes to hours) and multiphasic RNA folding (Zarrinkar and Williamson 1994; Sclavi et al. 1998; Swisher et al. 2002). Advances have been made in predicting RNA secondary and tertiary structures: Thermodynamic parameters have been measured for many motifs (Mathews and Turner 2006), and structure predictions have been interfaced with experimental techniques such as NMR (Hart et al. 2008) and SHAPE (Wilkinson et al. 2008; Deigan et al. 2009) to improve prediction of secondary structure. While the above studies contribute greatly to establishing physical principles of RNA folding, almost all have been conducted under "standard literature conditions" of dilute solution and folding-favorable nonphysiological ionic conditions of ~10 mM Mg^{2+} or 1 M Na^+/K^+.

Physiological conditions are quite different. Typical K^+ concentrations in prokaryotic and eukaryotic cells are only ~140 mM, while free Mg^{2+} concentrations are just 1.5–3.0 mM in prokaryotic cells (Lusk et al. 1968; Truong et al. 2013) and 0.5–1.0 mM in eukaryotic cells (London 1991; Alberts et al. 1994; Feig and Uhlenbeck 1999; Grubbs 2002; Romani 2007). Eukaryotic and prokaryotic cells also contain 20%–40% (w/v) macromolecules, as well as lower-

[3]**Corresponding author**
E-mail pcb5@psu.edu

Article published online ahead of print. Article and publication date are at http://www.rnajournal.org/cgi/doi/10.1261/rna.042747.113.

molecular-weight cosolutes, which can exclude volume, interact with the RNA, and lead to altered solvent properties (Ellis 2001; Minton 2001). Differences between standard literature folding conditions and in vivo folding conditions have the potential to profoundly affect RNA folding mechanisms, which is the focus of this study.

Steric crowding and variation of solvent properties via a variety of water-soluble neutral cosolutes, including polyethyleneglycol (PEG) and dextran, have been shown to affect, and in many cases promote, the stability and function of proteins (Zhou et al. 2008). These species also affect RNA folding. They promote ribozyme cleavage (Nakano et al. 2009; Strulson et al. 2012, 2013), drive compaction of large RNAs (Kilburn et al. 2010), and affect folding free energy (Spink and Chaires 1998; Lambert and Draper 2007; Spink et al. 2007; Feng et al. 2010; Denesyuk and Thirumalai 2011; Kilburn et al. 2013). While these studies provide insight into ways in which biological conditions affect RNA folding and function, there has been little focus on how they affect RNA folding cooperativity.

Folding of RNA is a largely hierarchical process (i.e., secondary then tertiary structure formation) (Brion and Westhof 1997; Leontis et al. 2006; Greenleaf et al. 2008) because most tertiary structure assembles from preformed secondary structures. For example, tRNA folds through five intermediates involving combinations of four different helices prior to formation of tertiary structure (Riesner et al. 1973; Crothers et al. 1974), while the HDV ribozyme folds through numerous base-pairing states and misfolds (Isambert and Siggia 2000; Chadalavada et al. 2002; Brown et al. 2004). Some variations in overall RNA folding mechanisms have been reported, e.g., tertiary structure or proteins driving native secondary structure (Thirumalai 1998; Wu and Tinoco 1998; Duncan and Weeks 2010; Woodson 2010); however, even in these cases, native secondary structure typically precedes tertiary structure. Although helical intermediates do exist in the folding pathway for functional RNAs, it remains unclear if they populate appreciably. Dill defined a cooperatively folding system as one in which obligate folding intermediates are poorly populated, or "hidden" (Ozkan et al. 2002; Weikl et al. 2004). If secondary structural helical intermediates are intrinsically unstable and only the initial and final states populate, then folding is defined as apparent two-state (all-or-none) and fully cooperative. On the other hand, a high population of intermediates leads to noncooperative folding (Kwok et al. 2013). In the present study, we probe the folding cooperativity of a functional RNA under biological solution conditions.

To assess the effects of molecular crowders and cosolutes on RNA folding cooperativity, we chose to study the folding of $tRNA^{Phe}$ (Fig. 1A). This choice was made for several reasons. First, the structure, folding, and function of tRNA has been characterized in the literature, with many studies detailing the folding of tRNA under standard literature folding conditions (Yang et al. 1972; Stein and Crothers 1976a,b; Fang et al. 2000; Misra and Draper 2000; Pulukkunat and Gopalan 2008). Second, tRNA has a well-folded native tertiary structure that is relevant to many functional RNAs in eukaryotic and prokaryotic cells. Third, the T7 transcript of tRNA has similar properties as the naturally occurring modified RNA (Sampson and Uhlenbeck 1988; Nobles et al. 2002; Wilkinson et al. 2005; Whitman 2011) but is easily mutated to provide weakened tertiary structure so that effects of molecular crowders and cosolutes on secondary and tertiary structure individually can be assessed (Fig. 1B). The tRNA chosen is unmodified $tRNA^{Phe}$ from yeast, which was selected because the base-pairing in the various helices has a relatively even distribution of GC and AU/GU base

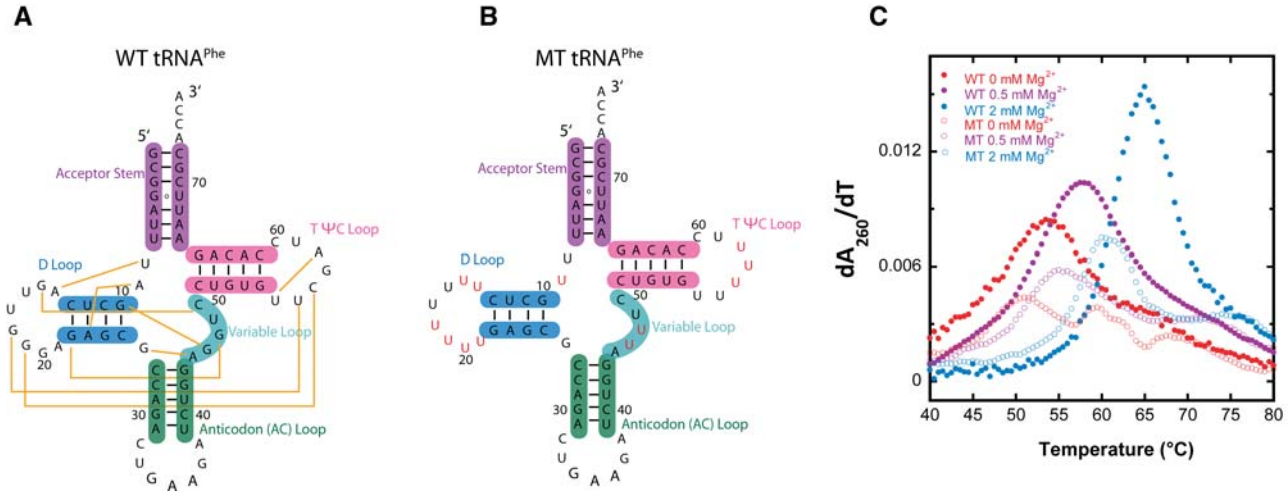

FIGURE 1. Secondary structure and first derivative melt curves of WT and MT $tRNA^{Phe}$. (*A*) Secondary structure of wild-type (WT) $tRNA^{Phe}$. WT $tRNA^{Phe}$ was prepared by in vitro T7 transcription. (*B*) Secondary structure of mutationally weakened tertiary structure $tRNA^{Phe}$, referred to as MT $tRNA^{Phe}$. (Red) Nucleotides mutated to remove tertiary contacts. (*C*) First derivative melt curves parameteric in Mg^{2+} concentration for WT $tRNA^{Phe}$ (closed symbols) and MT $tRNA^{Phe}$ (open symbols).

pairs. The latter was important so as not to bias the RNA toward or away from cooperative folding of secondary and tertiary structure.

Herein, we reveal that macromolecular crowding agents promote RNA folding cooperativity at biological concentrations of magnesium. Conversely, low-molecular-weight cosolutes either promote or diminish folding cooperativity in a manner dependent on the identity of the cosolute. We show that crowding agents promote cooperativity by stabilizing tertiary structure, while those low molecular cosolutes that promote cooperativity do so by stabilizing tertiary structure and/or destabilizing secondary structure. Temperature-dependent SHAPE analysis reveals RNA unfolding properties on a nucleotide basis and confirms increase in cooperativity in the presence of crowder and certain cosolutes.

RESULTS

Folding cooperativity of wild-type $tRNA^{Phe}$ in the absence of additives

We first evaluated the folding cooperativity of $tRNA^{Phe}$ in 0, 0.5, and 2 mM Mg^{2+} in the absence of crowding and cosolute additives, all in the background of 140 mM KCl. We chose to evaluate RNA folding in 0.5 and 2 mM Mg^{2+}, as these are within the range of free Mg^{2+} concentrations reported in eukaryotic and prokaryotic cells, respectively, and in 150 mM K^+, as this is near physiological (Lusk et al. 1968; London 1991; Alberts et al. 1994; Feig and Uhlenbeck 1999; Grubbs 2002; Romani 2007; Truong et al. 2013). Additionally, we examined folding in 140 mM KCl without Mg^{2+} added in order to later determine if molecular crowders and cosolutes could promote folding cooperativity in the absence of divalent ions.

We began by performing melts of the wild-type (WT) $tRNA^{Phe}$ in 0, 0.5, and 2 mM Mg^{2+} in the absence of additives. Melting data are provided in Figure 1C (closed symbols) and summarized in Table 1. In general, a cooperative melt is expected to display a sharpened two-state-like unfolding transition with the absence of shoulders, while a less cooperative or noncooperative melt is expected to display a broad unfolding transition where multiple shoulders may be observed. With no Mg^{2+} present, WT $tRNA^{Phe}$ has a broad melting profile that contains a noticeable shoulder and thus consists of at least two transitions (Fig. 1C). These properties are indicative of multiple folding intermediates and little to no folding cooperativity. This outcome is consistent with significant heterogeneity in the structure, which is expected with no divalent ions and only relatively low monovalent ions. In 0.5 mM Mg^{2+}, the major unfolding transition shifts to higher temperature, from 53.5°C to 57.5°C, and is sharpened, as evidenced by narrowing and heightening of the transition. Indeed, the max dA/dT of the derivative plot increases from 0.0084 to 0.0106 (Table 1); nonetheless, the transition is not highly cooperative, as evidenced in part by the long tail remaining in the transition (Fig. 1C). In the presence of 2 mM Mg^{2+}, there is just a single significant unfolding transition, which is noticeably cooperative when compared with the unfolding transitions in 0 and 0.5 mM Mg^{2+}. The unfolding transition is shifted to much higher temperatures, from 57.5°C in 0.5 mM Mg^{2+} to 65.0°C in 2 mM Mg^{2+}, and is much steeper, with a max dA/dT value of 0.0154 as compared with 0.0106 in 0.5 mM Mg^{2+}. These observations are consistent with earlier studies, which demonstrated that the unfolding of $tRNA^{fMet}$ is multistate at 0.5 mM Mg^{2+} but approximately two-state in 3 mM Mg^{2+} (Stein and Crothers 1976a).

Impact of macromolecular crowders on the folding cooperativity of wild-type $tRNA^{Phe}$

Having evaluated the impact of magnesium ion concentration on the folding of $tRNA^{Phe}$ in the absence of additives, we describe the effects of macromolecular crowders on RNA folding. We expected that the crowders would promote RNA folding cooperativity since they favor a more compact form of the RNA. The molecular crowders—PEG4000, PEG8000, Dextan10, Dextran70, and Ficoll70 with molecular weights of 4 kDa, 8 kDa, 8 kDa, 10 kDa, 70 kDa, and 70 kDa, respectively—were chosen because they allow exploration of different chemical compositions and sizes. Concentrations of these were 20% (w/v) to approximate the lower estimates of crowding in vivo (Minton 2001). Melting experiments on the WT $tRNA^{Phe}$ in the presence of the macromolecular crowders were performed at 0, 0.5, and 2 mM Mg^{2+}. These data are provided in Figure 2 both as a function of actual temperature and as a function of an offset temperature referred to as "T_{Buffer}," in which a constant was added to or subtracted from the actual temperature to give a T_m matched to the tRNA's T_m in buffer alone. This analysis was implemented to align the various melting maxima, facilitate comparison of melts, and aid generation of difference plots. Additionally, this treatment decouples thermostability and cooperativity, as they do not always parallel each other.

In the absence of magnesium, the crowding agents did not have a significant effect on folding cooperativity. For example, the max dA/dT in PEG8000 and Ficoll70 are somewhat lower than in buffer alone, while for PEG4000, Dextran10, and Dextran70, the max dA/dT values are slightly elevated above those in buffer alone (Fig. 2A; Table 1). The lack of any appreciable gains by the crowders on cooperativity in the absence of Mg^{2+} is visualized in the bar graphs in Figure 3A (left set of bars), where the max dA/dT for the first (i.e., lowest temperature) unfolding transition has been plotted as a function of additive.

Difference plots show melt data with additive present minus melt data in buffer alone and help reveal additive-specific effects (Fig. 4). For generation of these plots, the melt data as a function of T_{Buffer} were used. Difference melts in the absence of Mg^{2+} are relatively flat (Fig. 4A), consistent with a minimal effect on cooperativity in the absence of divalent ions. These plots are flat because the parent melts with and

TABLE 1. T_m and max *dA/dT* values for WT and MT $tRNA^{Phe}$ unfolding with increasing Mg^{2+} concentration

	WT $tRNA^{Phe}$			MT $tRNA^{Phe}$			
	T_m (°C)[a]	Max *dA/dT*[b]	Transitions[c]	T_m (°C)[a]	Max *dA/dT*[b]	Transitions[c]	
Buffer	53.5	0.0084	2	51.0	0.0048	3	0 mM Mg^{2+}
PEG4000	59.0	0.0091	1	55.0	0.0058	2	
PEG8000	60.0	0.0082	1	58.0	0.0062	2	
Dextran10	54.5	0.0095	2	52.5	0.0056	3	
Dextran70	53.5	0.0093	1	53.5	0.0045	3	
Ficoll70	56.5	0.0068	1	57.0	0.0061	3	
Methanol	53.5	0.0084	2	51.5	0.0068	2	
PEG200	53.0	0.0081	2	50.0	0.0064	2	
Proline	44.5	0.0073	2	41.0	0.0058	3	
TMAO	56.0	0.0085	2	56.5	0.0075	2	
Betaine	53.0	0.0097	2	49.0	0.0062	3	
	WT $tRNA^{Phe}$			MT $tRNA^{Phe}$			
	T_m (°C)[a]	Max *dA/dT*[b]	Transitions[c]	T_m (°C)[a]	Max *dA/dT*[b]	Transitions[c]	
Buffer	57.5	0.0106	1	55.0	0.0058	2	0.5 mM Mg^{2+}
PEG4000	62.0	0.0129	1	62.0	0.0070	2	
PEG8000	61.5	0.0125	1	63.0	0.0064	2	
Dextran10	59.0	0.0143	1	58.0	0.0064	2	
Dextran70	58.5	0.0122	1	59.5	0.0071	2	
Ficoll70	60.0	0.0108	1	59.5	0.0069	2	
Methanol	57.0	0.0124	1	56.0	0.0075	2	
PEG200	58.0	0.0149	1	54.5	0.0071	2	
Proline	47.0	0.0075	3	42.0	0.0062	3	
TMAO	59.0	0.0119	2	59.5	0.0077	3	
Betaine	53.5	0.0091	2	50.0	0.0070	2	
	WT $tRNA^{Phe}$			MT $tRNA^{Phe}$			
	T_m (°C)[a]	Max *dA/dT*[b]	Transitions[c]	T_m (°C)[a]	Max *dA/dT*[b]	Transitions[c]	
Buffer	65.0	0.0154	1	60.0	0.0075	2	2 mM Mg^{2+}
PEG4000	68.0	0.0182	1	65.5	0.0094	1	
PEG8000	69.0	0.0170	1	66.0	0.0083	1	
Dextran10	66.0	0.0181	1	63.5	0.0061	2	
Dextran70	67.0	0.0173	1	62.5	0.0054	2	
Ficoll70	66.5	0.0161	1	64.5	0.0077	2	
Methanol	64.5	0.0163	1	61.0	0.0080	2	
PEG200	64.5	0.0173	1	60.5	0.0080	2	
Proline	45.5	0.0077	3	44.5	0.0055	3	
TMAO	64.5	0.0152	1	61.5	0.0075	2	
Betaine	59.0	0.0135	1	54.0	0.0074	2	

[a]Typical errors in T_m are ±1°C (Sokoloski et al. 2011).
[b]The error in max *dA/dT* was no more than 10% based on comparison of duplicate measurements.
[c]The number of transitions was determined from the number of local maxima in the first derivative plots of the melts.

without additive (Fig. 2A, right panel) overlay very closely for 0 mM Mg^{2+}, with a small difference observed for Ficoll70.

In the presence of 0.5 mM Mg^{2+}, the crowding agents lead to a substantial increase in RNA folding cooperativity (Fig. 2B). Remarkably, every crowding agent tested led to an increase in the max *dA/dT* value from that of buffer alone (Fig. 3A; Table 1) and to sharpening of the folding transition. When melt data in the presence of additive were again offset to T_{Buffer}, it is evident that the crowder melts have higher *dA/dT* max than buffer alone (Fig. 2B, right panel). This effect is accentuated in the difference melts presented in Figure 4B, where there are distinct bell-shaped derivate plots in the presence of all crowders, with a positive node centered at the T_m in the presence of buffer denoted "$T_{m,Buffer}$." Additionally, there is a negative feature that precedes the positive node for several crowders leading to a so-called differential feature (Fig. 4B; Gong et al. 2008). The negative feature arises because the melting of the tRNA in the presence of the crowder is over a narrower temperature range, reflective of the sharpening of a transition as associated with RNA folding cooperativity.

In the presence of 2 mM Mg^{2+}, all crowders promote folding cooperativity (Fig. 2C). Every crowding agent again leads

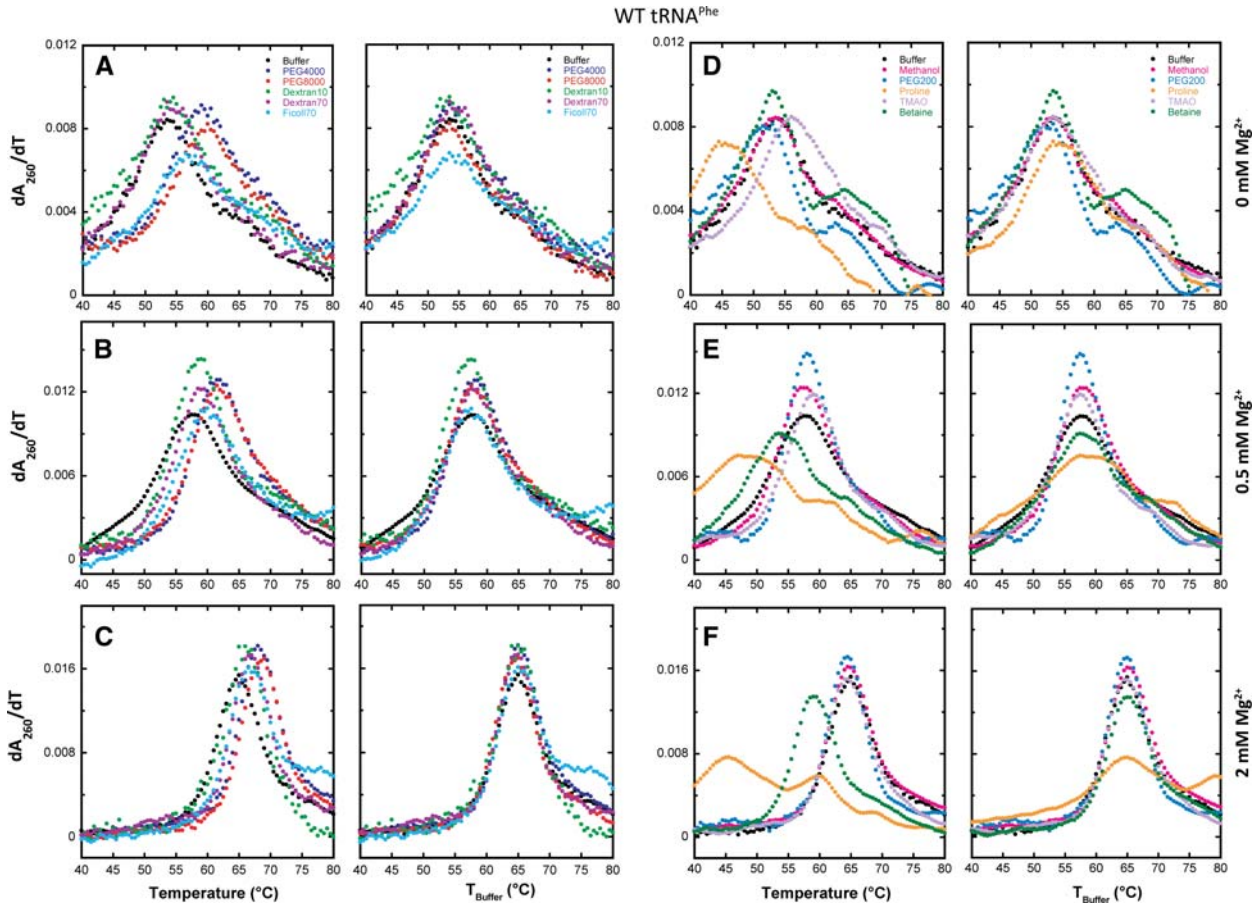

FIGURE 2. Melts of WT tRNA^{Phe} in additives with increasing Mg^{2+} concentration. All melts were performed in the background of 10 mM sodium cacodylate (pH 7.0) and 140 mM KCl. (*A–C*, both columns) The effects of various crowding agents (20% [w/v]) in 0, 0.5, and 2 mM Mg^{2+}, respectively. No additive (black), PEG4000 (blue), PEG8000 (red), Dextran10 (green), Dextran70 (purple), and Ficoll70 (cyan). (*D–F*, both columns) The effects of low-molecular-weight cosolutes (2 m, except PEG200, which was 20% [w/v]) in 0, 0.5, and 2 mM Mg^{2+}, respectively. No additive (black), methanol (pink), PEG200 (cobalt blue), proline (orange), TMAO (light purple), and betaine (dark green). In certain panels, data were adjusted to have the same T_m as the buffer, designated as "T_{Buffer}," so that the effects on cooperativity are clear.

to an increase in the value of max *dA/dT* over that in buffer alone (Fig. 3A; Table 1) and to sharpening of the folding transition. Examination of the difference melts in Figure 4C reveals bell-shaped derivative plots, similar to observations in 0.5 mM Mg^{2+}. Taken together, the 0.5 and 2 mM Mg^{2+} tRNA unfolding data indicate that biological magnesium concentrations allow folding cooperativity to be enhanced by crowding agents.

Next, we examined the apparent enthalpy change for the first unfolding transition in the melt because steeper (i.e., more cooperative) melting transitions are typically associated with greater enthalpy changes (Puglisi and Tinoco 1989). We fit the melting data to a two-state model to extract an apparent van't Hoff enthalpy, ΔH_{VH}. In several cases, the melting is clearly non-two-state, as discussed above; in these instances, we fit the first (i.e., lowest melting) apparent unfolding transition. The rationale for treating the data in

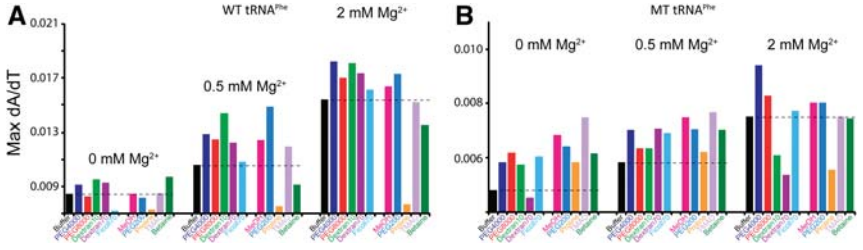

FIGURE 3. Max *dA*/*dT* plot of WT and MT tRNA^{Phe} with crowding and low-molecular-weight cosolute agents in increasing Mg^{2+} concentration. Max *dA*/*dT* values were calculated for the first (i.e., lowest temperature) unfolding transition from the first derivative melt curves for (*A*) WT and (*B*) MT. Experimental conditions and coloring of plots are identical to those in Figure 2. The black dashed line across each subset of conditions shows the max *dA*/*dT* in buffer alone for that condition. Bars that extend greater than the dashed line indicate an increase in folding cooperativity. Note the difference in the *y*-axis scales for panels *A* and *B*.

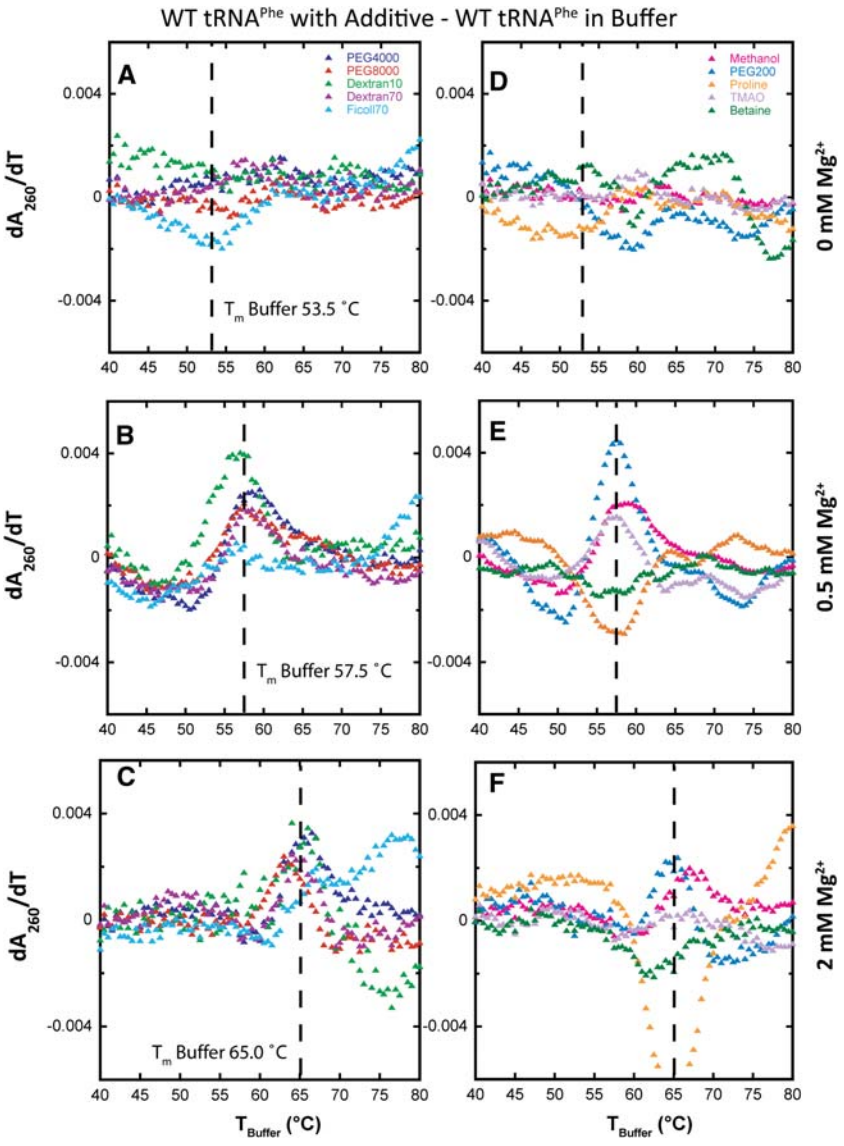

FIGURE 4. Difference plots of melts of WT tRNA^{Phe} in additives minus in buffer alone with increasing Mg^{2+} concentration. All melts were performed in the background of 10 mM sodium cacodylate (pH 7.0) and 140 mM KCl. All data were adjusted to have the same T_m, designated as "T_{Buffer}." (*A–C*) The effects of various crowding agents (20% [w/v]) in 0, 0.5, and 2 mM Mg^{2+}, respectively. PEG4000 (blue), PEG8000 (red), Dextran10 (green), Dextran70 (purple), and Ficoll70 (cyan). (*D–F*) The effects of low-molecular-weight cosolutes (2 m, except PEG200, which was 20% [w/v]) also in 0, 0.5, and 2 mM Mg^{2+}, respectively. Methanol (pink), PEG200 (cobalt blue), proline (orange), TMAO (light purple), and betaine (dark green). Difference plots show the effects of the additives on WT folding cooperativity.

this manner is that the apparent ΔH_{VH} from such a fit serves as a marker of the number of RNA interactions that unfold in the first transition and so describes in a semi-quantitative manner the degree of folding cooperativity. Values for ΔH_{VH} and $\Delta H_{VH}/\Delta H_{VH,buffer}$, which provide a comparison to buffer alone, are provided in Supplemental Table S1. In 0 mM Mg^{2+}, nearly all crowders led to a ΔH_{VH} for unfolding that is *smaller* in magnitude than in the absence of additive. This is revealed in relative $\Delta H_{VH}/\Delta H_{VH,buffer}$ factors that are less than unity, ranging from 0.7 to 0.8. These data provide no evidence for enhancement of folding cooperativity by the additive in the absence of Mg^{2+}, consistent with the analysis above.

We then extended this analysis to melts in the background of 0.5 mM Mg^{2+}. The value of ΔH_{VH} in the absence of additive increased from 39.7 to 47.6 kcal/mol upon increasing the Mg^{2+} from 0 to 0.5 mM, supporting a gain in folding cooperativity in the presence of 0.5 mM Mg^{2+} over no Mg^{2+}, consistent with the analysis above (Supplemental Table S1). Remarkably, in 0.5 mM Mg^{2+}, all of the crowders led to a ΔH_{VH} for unfolding that is *greater* in magnitude than in buffer alone, which is a trend opposite to that in the 0 mM Mg^{2+} background. This effect is clearly revealed in $\Delta H_{VH}/\Delta H_{VH,buffer}$ ratios that are substantially greater than unity, ranging from 1.1 to 1.4. This observation supports the above analysis that additives increase cooperativity in the background of 0.5 mM Mg^{2+}.

Evaluation of the 2 mM Mg^{2+} melt data reveals $\Delta H_{VH}/\Delta H_{VH,buffer}$ ratios that are greater than unity, again supporting the conclusion that most crowders promote cooperativity. The effect, however, is somewhat diminished relative to 0.5 mM Mg^{2+} effects, with maximal $\Delta H_{VH}/\Delta H_{VH,buffer}$ ratios near 1.1 rather than 1.4. This smaller effect may arise because the cooperativity has already been enhanced by the higher Mg^{2+}.

Impact of low-molecular-weight cosolutes on the folding cooperativity of wild-type tRNA^{Phe}

We next consider the effect of various low-molecular-weight cosolutes on RNA folding cooperativity. These measurements were conducted on tRNA^{Phe} in the same Mg^{2+} concentrations of 0, 0.5, and 2 mM Mg^{2+} in a background K^+ of 140 mM. Methanol, PEG200, proline, TMAO, and betaine were chosen for the low-molecular-weight cosolutes since they have been shown to stabilize or destabilize RNA, and in cases of proline, TMAO, and betaine are biologically relevant (Di Domenico and Lavecchia 2002; Lambert and Draper 2007; Nakano et al. 2009; Knowles et al. 2011). Concentrations of these were chosen to be 2 m, which is similar to concentrations used in other RNA folding studies (Lambert and Draper 2007).

We analyzed tRNA melting in the presence of cosolutes in 0, 0.5, and 2 mM Mg^{2+} (Fig. 2D). In the absence of Mg^{2+}, the small-molecule cosolutes do not have a significant effect on cooperativity, similar to that observed with the macromolecular crowders. For example, in the absence of added Mg^{2+}, the max *dA/dT* is quite similar in buffer alone and in each of the cosolutes with at least two transitions present in the presence of each cosolute (Table 1). This is also apparent in the plot of *dA/dT* maximum versus additive (Fig. 3A). In addition, the difference plots offset to the buffer-alone temperature show no distinct features (Fig. 4D), supporting no clear effect of cosolutes on folding cooperativity in the absence of divalent ions. We note that cosolutes lead both to increases and decreases in thermostability in the presence of the additive, which is distinct from the effect of macromolecular crowders, none of which decrease thermostability (Table 1).

In the presence of 0.5 mM Mg^{2+}, substantial effects of cosolute on RNA folding cooperativity are observed (Fig. 2E). As discerned from effects on the value of max *dA/dT*, PEG200, methanol, and TMAO all enhance folding cooperativity, while proline and betaine decrease folding cooperativity (Table 1, cf. max *dA/dT* values to buffer). These effects are especially apparent in the difference melts in Figure 4E. In the case of PEG200, methanol, and TMAO, their difference plots are bell-shaped with a positive feature centered at $T_{m,Buffer}$ and the max *dA/dT* greatest for PEG200. Moreover, the low-temperature negative differential feature is especially distinct for PEG200, which also shows a negative feature at higher temperature. The two negative features arise because melting of tRNA in the presence of PEG200 is especially sharp, reflecting enhanced folding cooperativity. In contrast, in proline and betaine, reverse effects are seen. The bell-shaped difference plots for betaine and especially proline are approximately mirror images of those for PEG200, methanol, and TMAO, in which the largest magnitude node is the negative node (Fig. 4E). This observation is consistent with a decrease in folding cooperativity arising from these additives. Last, in the presence of 2 mM Mg^{2+}, a gain in folding cooperativity still occurs upon addition of PEG200, methanol, and TMAO, but the stimulation is diminished from what it was in 0.5 mM Mg^{2+}, likely due to the same reasons discussed above for macromolecular crowders.

Consideration of enthalpy changes in the presence of cosolute strengthens the conclusions reached above. In particular, $\Delta H_{VH}/\Delta H_{VH,buffer}$ factors are ≤ 1 in the absence of Mg^{2+}, providing no evidence for cooperativity enhancement under these conditions (Supplemental Table S1). In the presence of 0.5 mM Mg^{2+}, $\Delta H_{VH}/\Delta H_{VH,buffer}$ factors range from 1.2 to 1.5 for PEG200, methanol, and TMAO, consistent with the abovementioned gains in folding cooperativity, while $\Delta H_{VH}/\Delta H_{VH,buffer}$ factors are 0.7 and 0.9 for proline and betaine, supporting the decrease in folding cooperativity in these cosolutes. In 2 mM Mg^{2+}, the $\Delta H_{VH}/\Delta H_{VH,buffer}$ factors are only 1.1–1.2 for PEG200, methanol, and TMAO, again consistent with smaller gains in folding cooperativity in higher Mg^{2+}. Proline and betaine ratios of $\Delta H_{VH}/\Delta H_{VH,buffer}$ remain similarly destabilizing at 0.6 and 0.9, respectively.

It is of interest to note that for the macromolecular crowders, increases in cooperativity were generally associated with increases in thermostability. For instance, thermostability increased in the presence of all crowders in 0, 0.5, and 2.0 mM Mg^{2+} by an average of 2.7°C, and by as much as 6.5°C. However, this trend does not hold for low-molecular-weight cosolutes, which had little or no effect on thermostability, except for proline and betaine, which decreased it. The differential effects of crowders and cosolutes on thermostability appear to be associated with their impacts on secondary and tertiary structure (see Discussion).

Finally, we conducted melts of tRNA in 10 mM Mg^{2+} in representative macromolecular crowders and low-molecular-weight cosolutes. These experiments were carried out in order to provide a comparison between the effects of physiological Mg^{2+} concentrations and folding-favorable, nonphysiological Mg^{2+} concentrations on RNA folding, as well as to test the effects of crowder and cosolute additives in these two Mg^{2+} backgrounds. These data can be found in Supplemental Figure S1. While crowders enhanced thermostability at biological Mg^{2+} concentrations, as discussed above, they had no appreciable effect on thermostability in the background of 10 mM Mg^{2+}. This is consistent with the notion that effects of additives are lessened in nonphysiologically high Mg^{2+} concentrations. On the other hand, the crowders did enhance folding cooperativity slightly in both Mg^{2+} concentrations.

Low molecular crowders had differential effects on thermostability at biological Mg^{2+}, as discussed above; however, they all decreased thermostability in the background of 10 mM Mg^{2+} (Supplemental Fig. S1). Likewise, while some cosolutes enhanced folding cooperativity and some decreased cooperativity at biological Mg^{2+} concentrations, in 10 mM Mg^{2+} slight enhancements or no effects on folding cooperativity were found. Overall, the effects of additives in 10 mM Mg^{2+} provide some biophysical insight for understanding how additives affect RNA folding; however, we focus herein on the effects of additives under biological Mg^{2+} concentrations.

Impact of crowders and cosolutes on the folding cooperativity of mutated tertiary $tRNA^{Phe}$

In an effort to dissect effects of additives on RNA secondary and tertiary structure formation, we prepared a mutated tertiary structure $tRNA^{Phe}$, referred to as MT, in which key tertiary interactions were abolished by changing D loop, variable loop, and TΨC loop residues to Us (Fig. 1B). The tertiary interactions targeted are represented by yellow lines in the WT secondary structure (Fig. 1A). The folding behavior of MT $tRNA^{Phe}$ was examined through perpendicular temperature-gradient gel electrophoresis (TGGE) (Bevilacqua and Bevilacqua 1998; Chadalavada and Bevilacqua 2009) displayed in Figure 5. The MT $tRNA^{Phe}$ migrates slower than

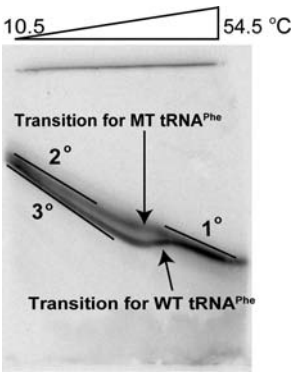

FIGURE 5. Perpendicular TGGE plot for WT and MT $tRNA^{Phe}$ melting transitions. Electrophoresis is 13% PAGE and 1× $THEN_{10}M_{0.9}$ (pH 7.5) (= 33 mM Tris, 66 mM HEPES, 0.1 mM EDTA, 10 mM NaCl, 0.9 mM $MgCl_2$) and 4 M urea (to facilitate melting in the TGGE range). Baselines slant to the *bottom right*-hand corner owing to the temperature gradient, which was also observed in the blue tracking dyes (data not shown).

WT at low temperatures, has a single lower-melting unfolding transition associated with loss of secondary structure, and then migrates identically to WT at higher temperatures. Slower migration than WT at low temperature is consistent with less compaction in MT and thus removal of much of the tertiary structure, while comigration with WT at high temperature supports identical unfolded structures for MT and WT.

We first tested MT $tRNA^{Phe}$ for any folding cooperativity by conducting melts in 0, 0.5, and 2 mM Mg^{2+} in the absence of additives in the background of 140 mM KCl (Fig. 1C, open symbols). In the absence of Mg^{2+}, MT $tRNA^{Phe}$ has a very broad melting profile that consists of at least three very distinct transitions with their own local maximum. In comparison to WT, MT $tRNA^{Phe}$ melts over a much wider temperature range and has a substantially smaller *dA/dT* maximum (0.0048 vs. 0.0084 for MT and WT, respectively) (Table 1). These observations clearly support multiple folding intermediates and absence of cooperativity.

When Mg^{2+} is added to a final concentration of 0.5 or 2 mM, the transitions shift to higher temperature, consistent with known effects of divalent ions on secondary structure (Fig. 1C; Serra et al. 2002). However, the melting profiles remain much broader than those in WT, show less thermostability, and contain multiple unfolding transitions. These results suggest that MT $tRNA^{Phe}$ does not fold with any significant cooperativity even in the presence of Mg^{2+}.

Next, we consider the effects of macromolecular crowders and low-molecular-weight cosolute additives on the folding of MT $tRNA^{Phe}$ in the presence of 0, 0.5, and 2 mM Mg^{2+}. The same additives at the same concentrations were studied as in WT $tRNA^{Phe}$. In the absence of Mg^{2+}, the crowding agents increase the max *dA/dT* relative to buffer (Fig. 6A). This change is not consistent with an increase in cooperativity, however, because the transition does not narrow and because two or three transitions are clearly evident (Table 1). Absence of narrowing is evident both in the similarity of the melts in the T_{Buffer} plots (Fig. 6A, right panel), as well as in the difference plots, which do not show a sharp feature (Fig. 7A); compare to Figure 4B, for example. Given that crowders are known to stabilize extended secondary structures but destabilize short secondary structures (Nakano et al. 2004), the increase in max *dA/dT* relative to buffer may be due to the cumulative effect of concomitantly melting secondary structural elements.

In the absence of Mg^{2+}, the cosolute agents show an even greater increase in the max *dA/dT* for MT $tRNA^{Phe}$ relative to buffer than do crowding agents (Fig. 6D). However, this change again is not consistent with an increase in cooperativity because the transition does not narrow and because two or three transitions are clearly evident (Table 1). Absence of narrowing is evidenced both in the similarity of the melts with and without cosolute in the T_{Buffer} plots (Fig. 6D, right panel) and the difference plots (Fig. 7D). Given that cosolutes are known to strongly destabilize secondary structure (Lambert and Draper 2007), the increase in max *dA/dT* for cosolutes relative to buffer for MT $tRNA^{Phe}$ may again be due to overlapping of the melting of many secondary structural elements.

In the presence of 0.5 mM Mg^{2+}, crowding additives have relatively little effect on the maximal value of *dA/dT* or the number of transitions, which remains at two or three (Fig. 6B; Table 1). Moreover, the difference melt plots show little or no regular features (Fig. 7B), consistent with little effect on folding cooperativity. Cosolutes again lead to an increase in max *dA/dT* relative to buffer, albeit by a smaller amount (Figs. 6E, 7E).

In the presence of 2 mM Mg^{2+}, there are more noticeable effects of crowders and cosolutes including a differential feature in the difference plots (Fig. 7C,F). The differential feature, however, has a *negative* node at $T_{m,Buffer}$, rather than a positive node as seen with WT (e.g., cf. Fig. 4B,E). Moreover, the positive node appears at a temperature *lower* than the $T_{m,Buffer}$. These features arise from broadening of the transition and are compatible with loss rather than gain of cooperativity. Observation that the number of unfolding transitions is two or three with most crowders and cosolutes (Table 1) further strengthens the conclusion that folding cooperativity of MT tRNA is not promoted by additives.

Last, we note that the thermostability of MT was affected by additives in a similar fashion as WT. Macromolecular crowders increased thermostability by an average of 4.7°C, while low molecular cosolutes had little or no effect on thermostability, with the same exceptions of proline and betaine.

Mapping of $tRNA^{Phe}$ structure by SHAPE as a function of temperature in the absence and presence of additives

The above thermodynamic results show that cooperativity of tRNA folding is induced by all macromolecular crowders

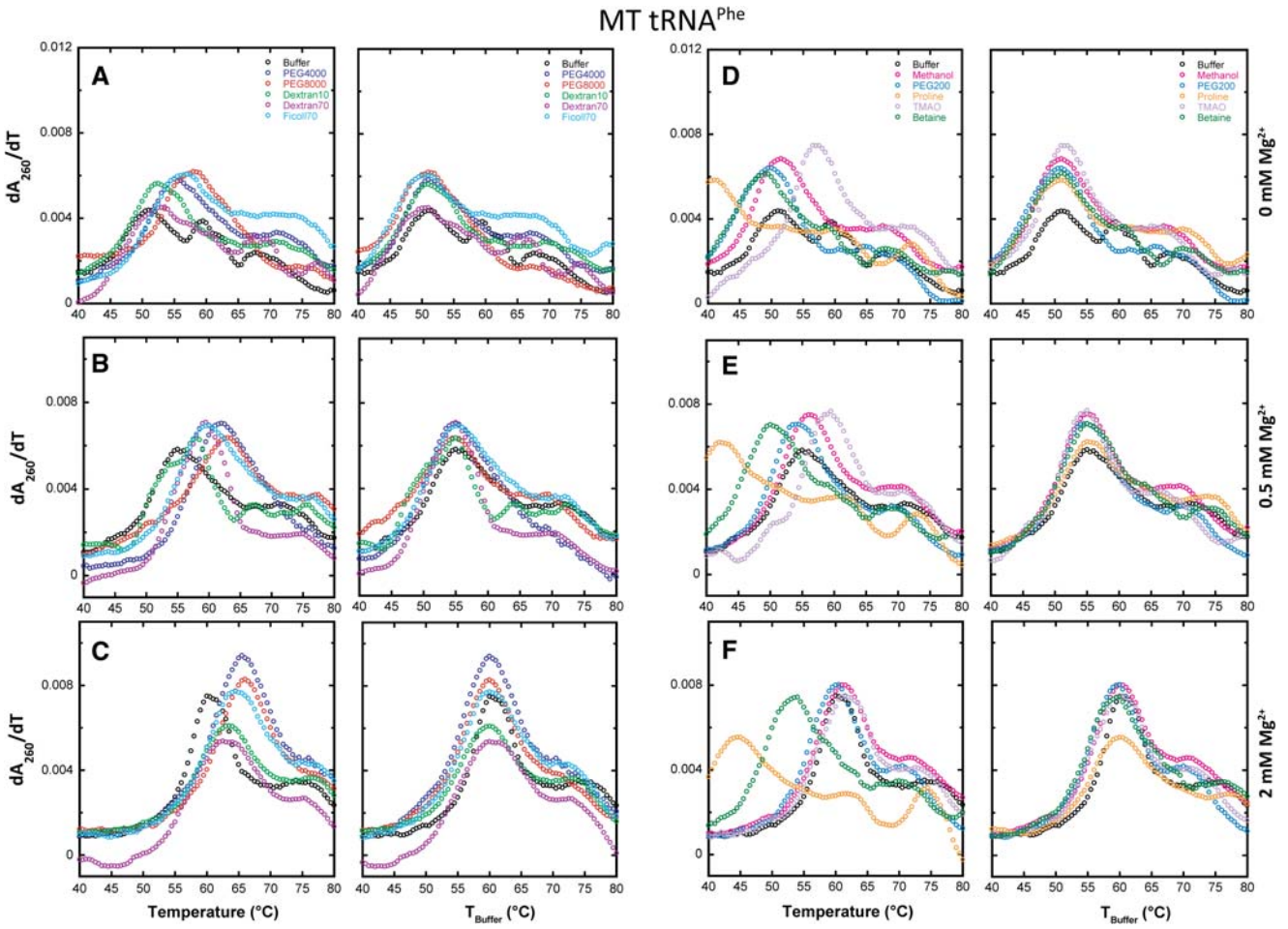

FIGURE 6. Melts of MT tRNA^{Phe} in additives with increasing Mg^{2+} concentration. All melts were performed in the background of 10 mM sodium cacodylate (pH 7.0) and 140 mM KCl. (*A–C*) The effects of various crowding agents (20% [w/v]) in 0, 0.5, and 2 mM Mg^{2+}, respectively. No additive (black), PEG4000 (blue), PEG8000 (red), Dextran10 (green), Dextran70 (purple), and Ficoll70 (cyan). (*D–F*) The effects of low-molecular-weight cosolutes (2 m, except PEG200, which was 20% [w/v]) in 0, 0.5, and 2 mM Mg^{2+}, respectively. No additive (black), methanol (pink), PEG200 (cobalt blue), proline (orange), TMAO (light purple), and betaine (dark green). In certain panels, data were adjusted to have the same T_m as the buffer, designated as "T_{Buffer}," so that the effects on cooperativity are clear.

tested as well as by certain low-molecular-weight crowders. To gain structural insight into these results, we assessed the structure of the tRNA by SHAPE in the absence and presence of PEG8000, methanol, and betaine, in the presence of 0.5 mM Mg^{2+}. The SHAPE method reagent acylates accessible and dynamic 2′-hydroxyls, which can be detected by reverse transcription (RT) (Merino et al. 2005; Wilkinson et al. 2006). We chose SHAPE because this method has been validated as providing detailed information on the secondary structure of folded RNAs under a wide range of conditions. To facilitate SHAPE experiments, a 30-nucleotide (nt) overhang was appended to the 3′ end of the tRNA to provide a primer binding site, with a 6-nt linker between the 3′ end of the tRNA and the extension (Supplemental Fig. S2B). This extension was designed not to interact with the tRNA, which was validated by free-energy minimization calculations as well as by the results presented below, which reveal a native fold to the tRNA^{Phe}. Structure mapping by SHAPE was done as a function of temperature every ~2.7°C between 41°C and 70°C, which spans the melting temperature. In terms of additives, we chose a macromolecular crowder and a cosolute that promoted cooperativity, as well as a cosolute that diminished cooperativity. PEG8000 was chosen as the crowder because it has an intermediate molecular weight and it should have minimal reactivity with the SHAPE reagent. Methanol was chosen as a cosolute to promote cooperativity, while betaine was chosen as a cosolute that diminished cooperativity. We tested 0.5 mM Mg^{2+} because the additives have the biggest effect of cooperativity under these conditions as described above.

We first mapped the structure of the tRNA^{Phe} in buffer alone and PEG8000 at 42.3°C, which is well below the T_m values in 0.5 mM Mg^{2+} in these conditions. SHAPE reactivity as a function of nucleotide position is provided in Supplemental Figure S2. SHAPE reactions in buffer alone and PEG8000 have nearly identical patterns under these

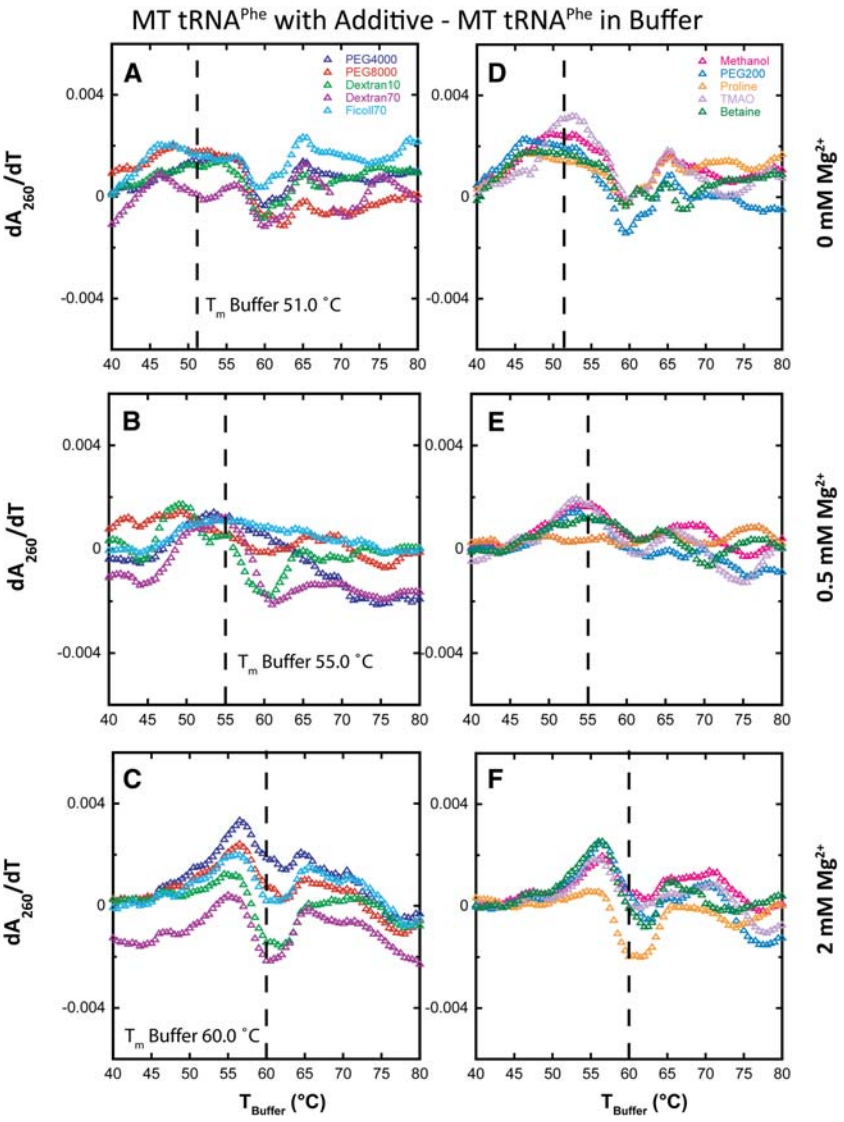

FIGURE 7. Difference plots of melts of MT tRNA^{Phe} in additives minus in buffer alone with increasing Mg^{2+} concentration. All melts were performed in the background of 10 mM sodium cacodylate (pH 7.0) and 140 mM KCl. All data were adjusted to have the same T_m, designated as "T_{Buffer}." (*A–C*) The effects of various crowding agents (20% [w/v]) in 0, 0.5, and 2 mM Mg^{2+}, respectively. PEG4000 (blue), PEG8000 (red), Dextran10 (green), Dextran70 (purple), and Ficoll70 (cyan). (*D–F*) The effects of low-molecular-weight cosolutes (2 m, except PEG200, which was 20% [w/v]) also in 0, 0.5, and 2 mM Mg^{2+}, respectively. Methanol (pink), PEG200 (cobalt blue), proline (orange), TMAO (light purple), and betaine (dark green). Difference plots show the effects of the additives on MT folding cooperativity.

conditions, with moderate to high reactivity in the D-loop, AC-loop, and TψC-loop regions, as well as in the linker region between the primer binding site and the 3′ end of the tRNA. These data were mapped onto the secondary structure of tRNA, as shown in Supplemental Figure S2, and agree with the established secondary and tertiary structure of tRNA. This result provides confirmation that this T7 transcript of tRNA^{Phe} folds natively in the presence of buffer and PEG8000 in 0.5 mM Mg^{2+}.

Next, SHAPE experiments were conducted as a function of temperature. We analyzed nucleotides in the D stem and loop, TψC loop, and acceptor stem. Nucleotides 25–32 (D stem and AC stem) were chosen because this stretch contains both secondary and tertiary structure; nucleotides 55–56 and 58 (TψC loop) were chosen because they participate only in tertiary interactions; and nucleotides 69 and 71–72 (acceptor stem) were chosen because they participate only in secondary interactions (Fig. 1A). Each of the nucleotide SHAPE temperature profiles was fit to a standard two-state melting equation, with sloping baselines as needed (see Materials and Methods).

As shown in Figure 8 (melts of individual nucleotides) and Supplemental Figure S3 (polyacrylamide gels), in the presence of buffer alone in 0.5 mM Mg^{2+}, the tRNA melts out in multiple transitions. For example, Figure 8A displays nucleotides that melt in the D stem and AC stem with T_ms ranging from 50.7°C to 60.9°C, while Figure 8B, C show nucleotides that melt in the TψC loop and acceptor stem with T_ms ranging from 48.8°C to 53.2°C. The T_m values observed span the T_m observed in UV melting in 0.5 mM Mg^{2+} and no additive of 57.5°C (Table 1). It is also noteworthy that some nucleotides transition from unmodified to modified to unmodified with increasing temperature, such as residue 55 in the TψC loop, supporting a population of a folding intermediate. Together, these data support low folding cooperativity in the presence of buffer alone, consistent with the UV-detected melting data.

In contrast to buffer alone, SHAPE data in the presence of 20% PEG8000 reveal that the tRNA melts out largely in a single transition. In this case, the same two-state transition was able to fit all the nucleotides in each of the above regions, with a T_m of ~61.6°C (Fig. 8D–F). Notably, the single T_m from each of these SHAPE-mapped regions agrees well with the T_m from the UV melts in 20% PEG8000 and 0.5 mM Mg^{2+} of 61.5°C (Table 1). Overall, the agreement among the T_m values derived from temperature-dependent SHAPE data for the different nucleotides in secondary and tertiary regions as well as the T_m from the UV melting experiments support the conclusion that

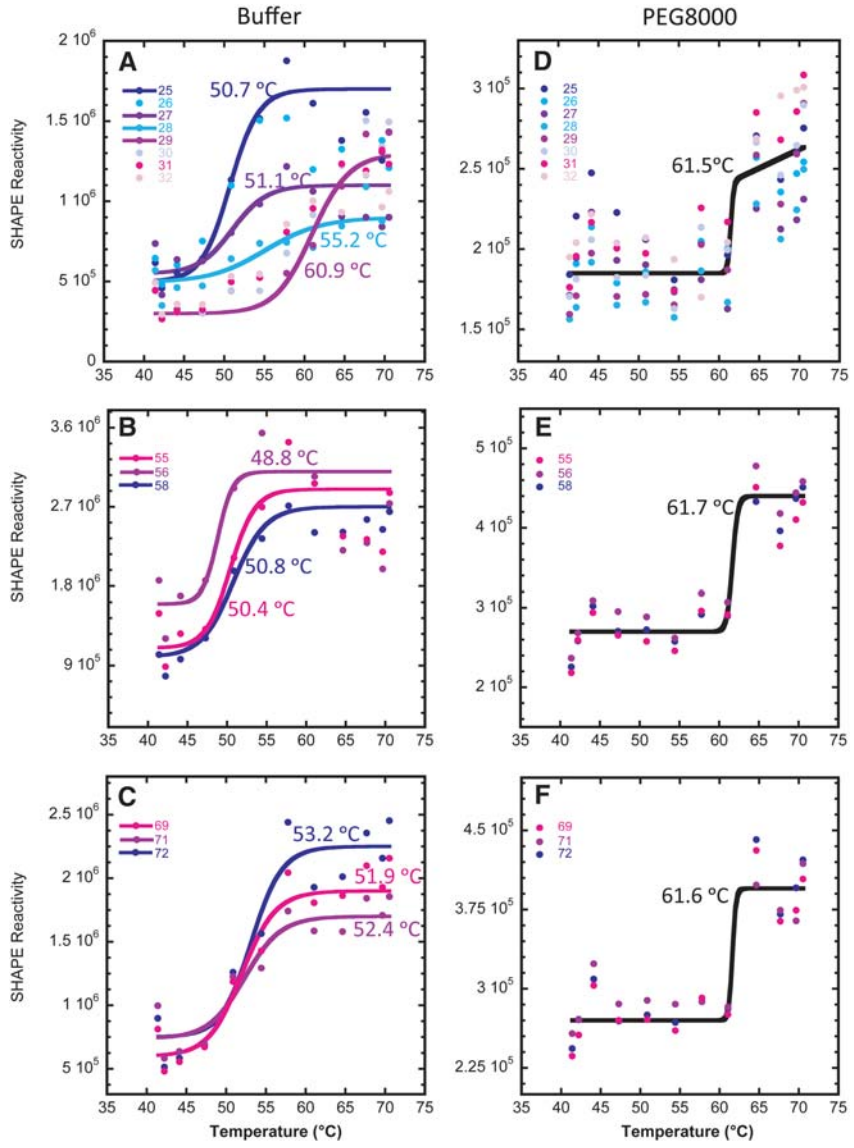

FIGURE 8. Temperature-dependent SHAPE analysis of WT $tRNA^{Phe}$ in the presence and absence of PEG8000 in 0.5 mM Mg^{2+}. (*A–C*) SHAPE analysis of WT $tRNA^{Phe}$ in buffer alone. (*D–F*) SHAPE analysis of WT $tRNA^{Phe}$ in 20% (w/v) PEG8000. (*A*,*D*) Nucleotides 25–32 in the D stem and AC stem (secondary and tertiary structure interactions). (*B*,*E*) Nucleotides 55, 56, and 58 in the TψC loop (tertiary structure interactions). (*C*,*F*) Nucleotides 69, 71, and 72 in the acceptor stem (secondary structure interactions). For plots *A–C* buffer alone, each nucleotide was fit separately to a two-state folding model, since there was poor correlation in T_ms for global analysis. For plots *D–F* in PEG8000, all nucleotides were fit globally since there was excellent agreement of T_ms within each data set and panel.

cooperativity is induced by addition of crowder in biological Mg^{2+}.

Next, we conducted SHAPE experiments on $tRNA^{Phe}$ at 42.3°C in the presence of either methanol or betaine, which is below their T_m values in 0.5 mM Mg (Supplemental Figs. S4, S5). The SHAPE reactivities were nearly identical in both additives, with reactivity primarily localized to the D-loop, AC-loop, and TψC-loop regions, as well as the linker region. These data mapped well onto the established secondary and tertiary structure of tRNA, indicating that this tRNA folds natively in the presence of both cosolutes in 0.5 mM Mg^{2+}. Mapping was then conducted as a function of temperature and plotted in the same regions of the tRNA described for buffer alone and PEG8000. In the presence of betaine, which is a destabilizing cosolute, the melting appears noncooperative (Supplemental Fig. S6). There is a pattern showing increased reactivity with temperature, followed by a decrease in reactivity, and followed by another increase in reactivity (Supplemental Fig. S6A–C). This pattern of reactivity is consistent with multiple unfolding transitions in certain regions of the RNA and suggests that the unfolding transition is noncooperative, which agrees with results from the melts. The temperature-dependent SHAPE reaction in the presence of betaine was therefore not fit to a two-state model.

In contrast, in the presence of methanol, which is a stabilizing cosolute, the melting appears cooperative (Supplemental Fig. S6). There is a pattern showing decreased reactivity with temperature, followed by an increase in reactivity, and followed by another decrease in reactivity. The decrease in reactivity with temperature is likely due to the SHAPE reagent 1M7 being consumed through reacting with methanol in an increasing fashion with temperature. In this case, the same two-state transition with negatively sloping baselines fits all the nucleotides in each of these three regions, and the thermodynamics parameters agree between the different regions with a T_m of ~60.2°C. This T_m is in reasonable agreement with the T_m from the melts of 57.0°C, especially given the difficulty in assigning baselines in the temperature-dependent SHAPE. In sum, the temperature-dependent SHAPE data in the presence of cosolutes agree well with the conclusions made from the UV melting experiments, which is that certain cosolutes, such as methanol, induced cooperative folding of the RNA, while others, such as betaine, diminish cooperative folding. Overall, the degree of cooperativity observed in the SHAPE analysis in the presence and absence of crowder and cosolutes parallels that inferred from the max *dA/dT* values of betaine < buffer < methanol < PEG8000 (Table 1), providing structural support to the above conclusions.

DISCUSSION

In this study, we examined the folding cooperativity of tRNA in the absence and presence of Mg^{2+}. The concentrations of Mg^{2+} tested, 0.5 and 2 mM, are similar to those typically found in eukaryotic and prokaryotic cells, respectively. Furthermore, we tested the effects of crowders and cosolutes on RNA folding cooperativity at concentrations typical of both cells. Melts revealed that increasing Mg^{2+} concentration increased RNA folding cooperativity, as expected, and that folding cooperativity is further enhanced in backgrounds of biological Mg^{2+} concentration by the presence of all macromolecular crowders tested. This was revealed in increased sharpness of single melting transitions. Melts in the presence of small-molecule cosolutes revealed that certain cosolutes, such as methanol and PEG200, increase folding cooperativity, whereas other cosolutes, such as betaine and proline, reduce folding cooperativity. Moreover, for those crowders and cosolutes that enhance cooperativity, the enhancements were similar in magnitude to the enhancements in going from no Mg^{2+} to 0.5 mM Mg^{2+}, as inferred from max *dA/dT* values. Probing the base-pairing status of individual nucleotides with SHAPE provided structural support for these conclusions, revealing enhanced cooperativity of tRNA folding in crowders and certain cosolutes in biological Mg^{2+} concentrations.

Origins of folding cooperativity and its relationship to thermostability

Folding cooperativity can be considered to arise from two limiting scenarios: (1) strengthening of tertiary structure interactions more than secondary structure interactions, or (2) weakening secondary structure interactions more than tertiary structure interactions. In this section, we consider the 0.5 mM Mg^{2+} data followed by 2 mM Mg^{2+}. In the absence of Mg^{2+}, essentially no cooperativity was observed, so this condition is not considered in detail.

The effects of crowders and cosolutes on WT and MT $tRNA^{Phe}$ thermostability and folding cooperativity in the presence of 0.5 mM Mg^{2+} are summarized in Scheme 1. In the presence of 0.5 mM Mg^{2+}, thermostability of both WT and MT $tRNA^{Phe}$ increased in various crowders relative to buffer alone (Table 1). However, the cooperativity of only WT $tRNA^{Phe}$ increased in the presence of crowder. Moreover, MT unfolded with at least two transitions but WT had one transition. Because thermostability increased for both WT and MT $tRNA^{Phe}$, with a somewhat greater increase for MT, it appears that the first scenario, in which tertiary structure interactions are strengthened more than secondary structure interactions, is responsible for the gain in folding cooperativity in the presence of crowders. Strengthening of tertiary structure is expected from the presence of macromolecular crowders (Nakano et al. 2009).

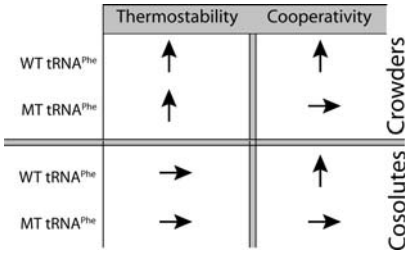

SCHEME 1. Summary of effects of cosolutes and crowders on thermostability and RNA folding cooperativity in the presence of eukaryotic free magnesium concentration of 0.5 mM Mg^{2+}. A vertical arrow signifies an increase, and a horizontal arrow signifies no change.

In general, the effects of cosolutes on cooperativity are specific to the given additive chosen. These effects of cosolutes on secondary structure stability are consistent with other results (Lambert and Draper 2007; Lambert et al. 2010), where TMAO was slightly stabilizing or destabilizing depending on the RNA, methanol was only slightly destabilizing, while proline and betaine were strongly destabilizing.

We first consider TMAO in the presence of 0.5 mM Mg^{2+}. Because TMAO both enhances folding cooperativity, as evidenced by a max *dA/dT* increase over buffer alone of 0.0106 to 0.0119, and thermostability, as evidenced by T_m increases from buffer alone for both WT and MT $tRNA^{Phe}$, it appears to enhance folding cooperativity by the first scenario in which tertiary structure interactions are strengthened more than secondary structure interactions.

Methanol and PEG200 both increase cooperativity, as evidenced by max *dA/dT* increases over buffer of 0.0106 to 0.0124 and 0.0149, respectively. In the presence of PEG200, which leads to the most cooperative unfolding, thermostability is enhanced in WT and diminished in MT, albeit by small effects. It thus appears that cooperativity arises in PEG200 due to a combination of both scenarios: strengthening of tertiary structure and weakening of secondary structure. It is likely the combination of these two mechanisms that leads to PEG200 being the additive that has the most cooperative unfolding. Studies on melting behavior of model oligonucleotides representing various $tRNA^{Phe}$ helices support this conclusion (data not shown), as do data on shorter oligonucleotides (Nakano et al. 2004). The molecular origin of this effect appears to be related to water activity being reduced in the presence of PEG200, which disfavors secondary structure formation but favors higher-order structure formation (Nakano et al. 2004; Knowles et al. 2011). With methanol, thermostability is changed only slightly in both the WT and MT, diminished in WT and enhanced in MT relative to buffer alone. The origin of the folding cooperativity increase in the presence of methanol thus appears to be related to increase in tertiary structure stability, which is consistent with other observations (Shiman and Draper 2000).

Proline and betaine both strongly destabilize thermostability, to the point where cooperativity is lost as revealed by max *dA/dT* decreases relative to buffer of 0.0106 to 0.0075 and 0.0091, respectively, and by the presence of multiple

transitions (Table 1). The origin of the loss of cooperativity could be due to interactions between the additive and the RNA and/or Mg^{2+} ions (Lambert and Draper 2007).

Next, we consider folding cooperativity in the presence of 2 mM Mg^{2+}. In the presence of crowders, thermostability of both WT and MT $tRNA^{Phe}$ increases relative to buffer alone, as in the case of 0.5 mM Mg^{2+}. Regarding cosolutes, folding cooperativity in 2 mM Mg^{2+} is still enhanced by PEG200 to a significant extent and by methanol to a smaller extent. Proline and betaine continue to diminish cooperativity, while TMAO no longer enhances cooperativity. Overall, cosolutes have similar, but not identical, effects on cooperativity in 2 and 0.5 mM Mg^{2+}. We do note, however, that the cooperativity gains in 2 mM Mg^{2+}, both in the presence of crowders and cosolutes, are somewhat smaller than those in 0.5 mM Mg^{2+}, as revealed by smaller gains in max *dA/dT*, in difference plots, and $\Delta H_{VH}/\Delta H_{VH,buffer}$. Diminished enhancement of cooperativity by additive is likely caused in large part because the background cooperativity in buffer alone is considerably greater in 2 mM Mg^{2+} than 0.5 mM Mg^{2+}. These results are qualitatively similar to those from Lambert and Draper, who observed that Mg^{2+} diminishes the stabilizing contributions of osmolytes for RNAs that bind Mg^{2+} diffusely (Lambert and Draper 2007).

Evidence that the unfolding of RNA is only partially cooperative

It appears that folding cooperativity gains in $tRNA^{Phe}$ are only partial. The largest ΔH for unfolding that we observe is ~100 kcal/mol, under conditions of 2 mM Mg^{2+} and all crowders as well as the cosolutes methanol, TMAO, and PEG200 (Supplemental Table S1). Turner rules suggest that melting of all the secondary structure should lead to a ΔH_{VH} for unfolding of ~208 kcal/mol (mFold with version 2.3 energies). Comparison of the ΔH values measured herein to those from Turner and coworkers is somewhat indirect as their melts are typically in 1 M NaCl, while ours are in 0.5 or 2.0 mM Mg^{2+} and 140 mM KCl, as well as the presence of various additives. Nonetheless, it appears that even in the more cooperative unfolding transitions observed herein, the extent of structure lost in the transition is not due to an all-or-none transition. Thus, while we clearly see that additives lead to increases in the magnitude of ΔH, it is likely the case that not all of the RNA is melting at once and that the gains in cooperativity are partial, at least under the conditions tested herein.

Weeks and colleagues conducted SHAPE studies on the folding of a different tRNA as a function of temperature (Wilkinson et al. 2005). Their experiments had several differences from ours, including studies based on a (unmodified) $tRNA^{Asp}$ from yeast, which is much more GC-rich than the yeast $tRNA^{Phe}$ studied herein, and a background of 10 mM Mg^{2+}. Nonetheless, they made a number of observations that are similar to ours. In particular, they found that certain tertiary structure and secondary structure elements melt simultaneously, while others melt separately. The similarities may come about because of the enhanced secondary structure stability from the GC-rich helices being offset by the enhanced tertiary structure stability from 10 mM Mg^{2+}.

CONCLUSIONS

Under standard literature conditions, intermolecular interactions in RNA are strong. For example, a helix of just 8 GC bp has a $t_{1/2}$ of ~16 h at 37°C and 1 M NaCl (Turner and Bevilacqua 1993). As such, RNA has the *potential* to be extraordinarily stable, with long-lived intermediates and misfolded intermediates. This has led to the notion that secondary structure is stronger than tertiary structure and that RNA folds through highly populated helical intermediates. This does not have to be the case, however. Base-pairing is typically much weaker in mesophilic than thermophilic functional RNAs (Galtier and Lobry 1997; Lu et al. 2006), and strong tertiary interactions can hold together intrinsically unstable helices (Stein and Crothers 1976a; Blose et al. 2007). Thus, it is possible that secondary and tertiary structure could melt simultaneously leading to partial or full unfolding cooperativity.

Herein, we established that physiological concentrations of crowding and cosolutes influence the folding cooperativity of RNA in biological Mg^{2+} concentrations. Future studies will be needed to dissect the molecular identity of the cooperativity through such methods as double and triple mutant cycles (Siegfried and Bevilacqua 2009), which we and others have applied under dilute solution conditions (Moody and Bevilacqua 2003; Moody et al. 2004; Sattin et al. 2008; Behrouzi et al. 2012). Moreover, studies will be needed on large, multidomain RNAs to see if these respond differently to crowders and cosolutes. In addition, studies will be needed to probe the extent of folding cooperativity in living cells to determine if RNA folds cooperatively, paralleling protein folding under these conditions.

MATERIALS AND METHODS

Chemicals

PEG4000 was from Alfa Aesar; PEG8000 was from Research Organics; PEG200, proline, TMAO, betaine, Dextran10, Dextran70, and Ficoll70 were from Sigma-Aldrich; methanol was from Mallinckrodt. $MgCl_2$ was obtained from J.T. Baker; KCl was from EMD Chemicals; and sodium cacodylate was from Sigma-Aldrich. 1M7 was a gift from the Showalter laboratory. Polynucleotide kinase was from New England Biolabs. SuperScript III reverse transcriptase was from Invitrogen.

RNA preparation

All $tRNA^{Phe}$ substrates were prepared by in vitro T7 transcription using 10% T7 RNA polymerase in 40 mM Tris (pH 8.0), 25 mM $MgCl_2$,

2 mM DTT, 1 mM spermidine, and 4 mM NTPs for 4 h at 37°C. The RNA was purified by 10% PAGE and recovered by a crush-and-soak, ethanol precipitation procedure. DNA oligonucleotide templates to make T7 $tRNA^{Phe}$ were purchased from Integrated DNA Technologies (IDT) and used without further purification.

The sequences of tRNA are as follows:

Wild-type $tRNA^{Phe}$, 5′-GCGGAUUUAGCUCAGUUGGGAGAGC GCCAGACUGAAGAUCUGGAGGUCCUGUGUUCGAUCCA CAGAAUUCGCACCA;
Mutated tertiary (MT) $tRNA^{Phe}$, 5′-GCGGAUUUUGCUCUUUU UUUUGAGCGCCAGACUGAAGAUCUGGAUUUCCUGUGU UUUUUCCACAGAAUUCGCACCA;
SHAPE $tRNA^{Phe}$, 5′-GCGGAUUUAGCUCAGUUGGGAGAGCG CCAGACUGAAGAUCUGGAGGUCCUGUGUUCGAUCCAC AGAAUUCGCACCAAGAAAACCAAAUCGGGCUUCGGUCC GGUUC.

WT and MT $tRNA^{Phe}$ were exchanged into 10 mM sodium cacodylate (pH 7.0) buffer using an Amicon Ultracentrifugal filter (MWCO, 3 kDa).

RNA thermal denaturation monitored by UV absorbance

WT and MT $tRNA^{Phe}$ were first renatured by heating for 3 min to 90°C in buffer and KCl and cooled to room temperature over 10 min. The final concentration of RNA in all melts was 0.5 μM. The $MgCl_2$ was then added to RNA, and the samples were heated for 3 min to 55°C and cooled to room temperature over 10 min. The $MgCl_2$ was not included in the high-temperature renaturation to avoid cleavage to the RNA backbone. Crowder or low-molecular-weight cosolute was added during the second renaturation step with the Mg^{2+}. Following addition of the Mg^{2+} and/or crowding or cosolute agent, the sample was centrifuged at 16,000*g* for 10 min to degas the sample.

All crowding and cosolute agents were prepared as 2× stock solutions and centrifuged at 16,000*g* for 20 min after preparation. Macromolecular crowding agents (PEG4000, PEG8000, Dextran10, Dextran70, and Ficoll70) were present at a final concentration of 20% (w/v), and low-molecular-weight cosolutes (methanol, PEG200, proline, TMAO, and betaine) were present at a final concentration of 2 m, with the exception of PEG200, which was present at 20% (w/v). Melting experiments were performed in the background of 10 mM sodium cacodylate (pH 7.0) and 140 mM KCl with either 0, 0.5, or 2 mM $MgCl_2$. A Gilford Response II spectrophotometer was used for melting experiments, with a data point acquired every 0.5°C and a heating rate of ~0.6°/min at 260 nm. All melts were performed in duplicate, and excellent agreement between these melts was observed.

Melts of all WT and MT $tRNA^{Phe}$ transcripts were normalized by dividing all absorbance readings by the maximum absorbance value. Monophasic melt data were fit to a two-state model using sloping baselines and analyzed using a Marquadt algorithm for nonlinear curve fitting in KaleidaGraph v. 3.5 (Synergy software) (Siegfried and Bevilacqua 2009). Since excellent agreement in melts was observed in duplicate measurements, only one melt from each trial was used for data analysis. Errors from these fits are reported. Derivative plots were of normalized data and were smoothed using an 11-point window prior to taking the derivative. T_m values were calculated by identifying the max *dA/dT* in the derivative plot; when multiple maxima were present, the reported T_m and max *dA/dT* are for the first transition, which involves tertiary structure and also had the largest *dA/dT*. T_m values for subsequent transitions are not reported as these are likely due to contributions of multiple transitions. The number of transitions reported in Table 1 is equal to the number of local maxima. All difference plots were generated from normalized melt curves.

Temperature gradient gel electrophoresis

Electrophoresis was performed in 13% polyacrylamide, 1× $THEN_{10}M_{0.9}$ (pH 7.5) (33 mM Tris, 66 M HEPES, 0.1 mM EDTA, 10 mM NaCl, 0.9 mM $MgCl_2$), and a semi-denaturing background of 4 M urea in order to facilitate melting in the TGGE temperature range (Bevilacqua and Bevilacqua 1998; Chadalavada and Bevilacqua 2009). Briefly, the experiment was conducted in perpendicular format in which samples were layered across a single wide well to which a temperature gradient of ~10°C–60°C was applied. The temperature was measured directly in the gel using a digital thermometer and a long narrow probe. The gel was then dried and imaged on the PhosphorImager. Melting temperatures were determined graphically by interpolation, and comparisons between T_ms were carried out for samples fractionated on the same gel. WT and MT were loaded at different concentrations to allow traces to be assigned.

Temperature-dependent SHAPE

The SHAPE $tRNA^{Phe}$ transcript was prepared as described above. The sequence of the RNA was identical to the WT $tRNA^{Phe}$ but contained a 3′-extension AGAAAACCAAAUCGGGCUUCGGUCCGG UUC-3′, which provided a 6-nt spacer (AGAAAA) and a binding site for the RT primer. Free-energy minimization calculations with mFold (Zuker 2003) supported absence of interaction of this extension with the tRNA itself, which was further supported by the SHAPE results reported herein. The RT primer (IDT, HPLC purified) was labeled on its 5′ end with [γ-^{32}P]ATP and polynucleotide kinase. The labeled primer was purified using a GE Healthcare G-50 microspin column to remove unincorporated ATP.

The WT $tRNA^{Phe}$ sample for SHAPE analysis was diluted to a final concentration of 150 nM in buffer conditions of 100 mM HEPES (pH 7.6)/0.5 mM Mg^{2+}/100 mM KCl. Temperature-dependent SHAPE was performed in 0.5 mM Mg^{2+} both with and without additives, and each had a total reaction volume of 20 μL. RNA was first renatured by heating for 1 min to 90°C in buffer and KCl only, and then cooled to room temperature over 2 min. The $MgCl_2$ was then added to the RNA, and the samples were heated for 2 min to 55°C. Samples were cooled to room temperature for 2 min during which time the additive was added, and then incubated for 1 min at 4°C. PEG8000 was present at a final concentration of 20% (w/v), and betaine and methanol were present at a final concentration of 2 m to mirror melting experiments. All heating and cooling were performed on a Biometra Tcycler thermocycler. Samples were then brought to the temperature of the experiment and incubated at that temperature for 2 min prior to addition of the SHAPE reagent to ensure that the sample had reached that temperature. A temperature window of 41°C–70°C was used with an ~2.7°C temperature step between wells. Temperature in the gradient cycler was calibrated using a thermocouple.

The chemical probing step of SHAPE was performed similar to that previously described (Wilkinson et al. 2006; Gherghe et al. 2008). Briefly, the electrophile 1M7 (dissolved in DMSO) was diluted to a final concentration of ~10 mM to allow single-hit kinetics conditions (Gherghe et al. 2008). Reactions were carried out for 2 min for the lower temperature samples and 1 min for the higher temperature samples, which allowed for ~5 half-lives of the 1M7 reagent. An experiment containing no SHAPE reagent was also performed, and it was found that the background reaction is not highly temperature dependent (Supplemental Fig. S7). Ethanol was added after reactions were complete, and the tubes were immediately placed on dry ice for precipitation. Reverse transcription was then performed for 10 min at 55°C, using SuperScript III (Invitrogen) along with dideoxy sequencing. Next, RNA was hydrolyzed by addition of 0.5 µL of 2 M NaOH and heating for 1 min at 95°C. Equal volume of formamide loading buffer was added, and samples were fractionated on a denaturing 10% polyacrylamide gel. Gels were visualized using a PhosphorImager and analyzed using ImageQuant software (Molecular Dynamics).

SHAPE data analysis

SHAPE data were first analyzed to assess the overall fold of the $tRNA^{Phe}$. This analysis was performed for SHAPE reactions in the presence and absence of additives to test whether the additives altered the native fold of the RNA. For these plots, the overall fold of the RNA was determined at 42.3°C. Background reaction (RT stops without SHAPE reagent present) was subtracted from the buffer alone and additive SHAPE reactions. Data were normalized using SAFA before subtraction for these plots (Das et al. 2005). These data were normalized to the most intense nucleotide on the gel, excluding the full-length band, following subtraction of the no SHAPE reagent reaction.

For analysis of temperature-dependent SHAPE data, the plotted regions were chosen to represent a diverse set of RNA motifs. All data are under single-hit conditions, as judged by the large amount of full-length band at the top of the SHAPE gels. To account for loading differences on the gel, differences in yield of RNA following precipitation and temperature dependence of the SHAPE reagent, the data were normalized to nucleotides 34–36 in the anticodon loop, as these nucleotides are single-stranded throughout the temperature range. The data were fit to a two-state melting model using either a sloping or nonsloping baseline depending on the data (Siegfried and Bevilacqua 2009). A Marquadt algorithm for nonlinear curve fitting in KaleidaGraph v. 3.5 (Synergy software) was used. Baselines were assigned by minimizing the error in the fit. When possible the folding of multiple nucleotides was fit to a single set of thermodynamic parameters corresponding to a two-state transition; otherwise, data were fit separately to two-state transitions.

SUPPLEMENTAL MATERIAL

Supplemental material is available for this article.

ACKNOWLEDGMENTS

We thank Kaycee Quarles, Chris Wostenberg, and Scott Showalter for providing the SHAPE reagent as a gift. We also thank Chun Kit Kwok and Rao Nallagatla for their assistance in SHAPE and TGGE experiments, and Christine Keating for helpful discussions. This work was supported by NASA grant NNX13AI01G.

Received September 28, 2013; accepted November 22, 2013.

REFERENCES

Alberts B, Bray D, Lewis J, Raff M, Roberts K, Watson JD. 1994. *Molecular biology of the cell*, 3rd ed. Garland Science, New York.

Behrouzi R, Roh JH, Kilburn D, Briber RM, Woodson SA. 2012. Cooperative tertiary interaction network guides RNA folding. *Cell* **149:** 348–357.

Bevilacqua JM, Bevilacqua PC. 1998. Thermodynamic analysis of an RNA combinatorial library contained in a short hairpin. *Biochemistry* **37:** 15877–15884.

Blose JM, Silverman SK, Bevilacqua PC. 2007. A simple molecular model for thermophilic adaptation of functional nucleic acids. *Biochemistry* **46:** 4232–4240.

Brion P, Westhof E. 1997. Hierarchy and dynamics of RNA folding. *Annu Rev Biophys Biomol Struct* **26:** 113–137.

Brown TS, Chadalavada DM, Bevilacqua PC. 2004. Design of a highly reactive HDV ribozyme sequence uncovers facilitation of RNA folding by alternative pairings and physiological ionic strength. *J Mol Biol* **341:** 695–712.

Chadalavada DM, Bevilacqua PC. 2009. Analyzing RNA and DNA folding using temperature gradient gel electrophoresis (TGGE) with application to in vitro selections. *Methods Enzymol* **468:** 389–408.

Chadalavada DM, Senchak SE, Bevilacqua PC. 2002. The folding pathway of the genomic hepatitis δ virus ribozyme is dominated by slow folding of the pseudoknots. *J Mol Biol* **317:** 559–575.

Crothers DM, Cole PE, Hilbers CW, Shulman RG. 1974. The molecular mechanism of thermal unfolding of *Escherichia coli* formylmethionine transfer RNA. *J Mol Biol* **87:** 63–88.

Das R, Laederach A, Pearlman SM, Herschlag D, Altman RB. 2005. SAFA: Semi-automated footprinting analysis software for high-throughput quantification of nucleic acid footprinting experiments. *RNA* **11:** 344–354.

Deigan KE, Li TW, Mathews DH, Weeks KM. 2009. Accurate SHAPE-directed RNA structure determination. *Proc Natl Acad Sci* **106:** 97–102.

Denesyuk NA, Thirumalai D. 2011. Crowding promotes the switch from hairpin to pseudoknot conformation in human telomerase RNA. *J Am Chem Soc* **133:** 11858–11861.

Di Domenico R, Lavecchia R. 2002. Stabilization of human haemoglobin by naturally occurring osmolytes. *Biochem Eng J* **10:** 27–30.

Duncan CD, Weeks KM. 2010. Nonhierarchical ribonucleoprotein assembly suggests a strain-propagation model for protein-facilitated RNA folding. *Biochemistry* **49:** 5418–5425.

Ellis RJ. 2001. Macromolecular crowding: Obvious but underappreciated. *Trends Biochem Sci* **26:** 597–604.

Fang X, Littrell K, Yang X, Henderson SJ, Siefert S, Thiyagarajan P, Pan T, Sosnick TR. 2000. Mg^{2+}-dependent compaction and folding of yeast $tRNA^{Phe}$ and the catalytic domain of the *B. subtilis* RNase P RNA determined by small-angle X-ray scattering. *Biochemistry* **39:** 11107–11113.

Feig AL, Uhlenbeck OC. 1999. The role of metal ions in RNA biochemistry. In *The RNA world* (ed. Gesteland RF, Cech TR, Atkins JF), pp. 287–319. Cold Spring Harbor Laboratory Press, Cold Spring Harbor, NY.

Feng B, Frykholm K, Norden B, Westerlund F. 2010. DNA strand exchange catalyzed by molecular crowding in PEG solutions. *Chem Commun* **46:** 8231–8233.

Galtier N, Lobry JR. 1997. Relationships between genomic G + C content, RNA secondary structures, and optimal growth temperature in prokaryotes. *J Mol Evol* **44:** 632–636.

Gherghe CM, Mortimer SA, Krahn JM, Thompson NL, Weeks KM. 2008. Slow conformational dynamics at C2′-endo nucleotides in RNA. *J Am Chem Soc* **130:** 8884–8885.

Gong B, Chen Y, Christian EL, Chen JH, Chase E, Chadalavada DM, Yajima R, Golden BL, Bevilacqua PC, Carey PR. 2008. Detection of innersphere interactions between magnesium hydrate and the phosphate backbone of the HDV ribozyme using Raman crystallography. *J Am Chem Soc* **130:** 9670–9672.

Greenleaf WJ, Frieda KL, Foster DA, Woodside MT, Block SM. 2008. Direct observation of hierarchical folding in single riboswitch aptamers. *Science* **319:** 630–633.

Grubbs RD. 2002. Intracellular magnesium and magnesium buffering. *Biometals* **15:** 251–259.

Hart JM, Kennedy SD, Mathews DH, Turner DH. 2008. NMR-assisted prediction of RNA secondary structure: Identification of a probable pseudoknot in the coding region of an R2 retrotransposon. *J Am Chem Soc* **130:** 10233–10239.

Isambert H, Siggia ED. 2000. Modeling RNA folding paths with pseudoknots: Application to hepatitis δ virus ribozyme. *Proc Natl Acad Sci* **97:** 6515–6520.

Kilburn D, Roh JH, Guo L, Briber RM, Woodson SA. 2010. Molecular crowding stabilizes folded RNA structure by the excluded volume effect. *J Am Chem Soc* **132:** 8690–8696.

Kilburn D, Roh JH, Behrouzi R, Briber RM, Woodson SA. 2013. Crowders perturb the entropy of RNA energy landscapes to favor folding. *J Am Chem Soc* **135:** 10055–10063.

Knowles DB, LaCroix AS, Deines NF, Shkel I, Record MT. 2011. Separation of preferential interaction and excluded volume effects on DNA duplex and hairpin stability. *Proc Natl Acad Sci* **108:** 12699–12704.

Kwok CK, Sherlock ME, Bevilacqua PC. 2013. Decrease in RNA folding cooperativity by deliberate population of intermediates in RNA G-quadruplexes. *Angew Chem Int Ed* **52:** 683–686.

Lambert D, Draper DE. 2007. Effects of osmolytes on RNA secondary and tertiary structure stabilities and RNA–Mg^{2+} interactions. *J Mol Biol* **370:** 993–1005.

Lambert D, Leipply D, Draper DE. 2010. The osmolyte TMAO stabilizes native RNA tertiary structures in the absence of Mg^{2+}: Evidence for a large barrier to folding from phosphate dehydration. *J Mol Biol* **404:** 138–157.

Leontis NB, Lescoute A, Westhof E. 2006. The building blocks and motifs of RNA architecture. *Curr Opin Struct Biol* **16:** 279–287.

London RE. 1991. Methods for measurement of intracellular magnesium: NMR and fluorescence. *Annu Rev Physiol* **53:** 241–258.

Lu ZJ, Turner DH, Mathews DH. 2006. A set of nearest neighbor parameters for predicting the enthalpy change of RNA secondary structure formation. *Nucleic Acids Res* **34:** 4912–4924.

Lusk JE, Williams RJ, Kennedy EP. 1968. Magnesium and the growth of *Escherichia coli*. *J Biol Chem* **243:** 2618–2624.

Mathews DH, Turner DH. 2006. Prediction of RNA secondary structure by free energy minimization. *Curr Opin Struct Biol* **16:** 270–278.

Merino EJ, Wilkinson KA, Coughlan JL, Weeks KM. 2005. RNA structure analysis at single nucleotide resolution by selective 2′-hydroxyl acylation and primer extension (SHAPE). *J Am Chem Soc* **127:** 4223–4231.

Minton AP. 2001. The influence of macromolecular crowding and macromolecular confinement on biochemical reactions in physiological media. *J Biol Chem* **276:** 10577–10580.

Misra VK, Draper DE. 2000. Mg^{2+} binding to tRNA revisited: The nonlinear Poisson–Boltzmann model. *J Mol Biol* **299:** 813–825.

Moghaddam S, Caliskan G, Chauhan S, Hyeon C, Briber RM, Thirumalai D, Woodson SA. 2009. Metal ion dependence of cooperative collapse transitions in RNA. *J Mol Biol* **393:** 753–764.

Moody EM, Bevilacqua PC. 2003. Folding of a stable DNA motif involves a highly cooperative network of interactions. *J Am Chem Soc* **125:** 16285–16293.

Moody EM, Feerrar JC, Bevilacqua PC. 2004. Evidence that folding of an RNA tetraloop hairpin is less cooperative than its DNA counterpart. *Biochemistry* **43:** 7992–7998.

Nakano S, Karimata H, Ohmichi T, Kawakami J, Sugimoto N. 2004. The effect of molecular crowding with nucleotide length and cosolute structure on DNA duplex stability. *J Am Chem Soc* **126:** 14330–14331.

Nakano S, Karimata HT, Kitagawa Y, Sugimoto N. 2009. Facilitation of RNA enzyme activity in the molecular crowding media of cosolutes. *J Am Chem Soc* **131:** 16881–16888.

Nobles KN, Yarian CS, Liu G, Guenther RH, Agris PF. 2002. Highly conserved modified nucleosides influence Mg^{2+}-dependent tRNA folding. *Nucleic Acids Res* **30:** 4751–4760.

Ozkan SB, Dill KA, Bahar I. 2002. Fast-folding protein kinetics, hidden intermediates, and the sequential stabilization model. *Protein Sci* **11:** 1958–1970.

Puglisi JD, Tinoco I. 1989. Absorbance melting curves of RNA. *Methods Enzymol* **180:** 304–325.

Pulukkunat DK, Gopalan V. 2008. Studies on *Methanocaldococcus jannaschii* RNase P reveal insights into the roles of RNA and protein cofactors in RNase P catalysis. *Nucleic Acids Res* **36:** 4172–4180.

Riesner D, Maass G, Thiebe R, Philippsen P, Zachau HG. 1973. The conformational transitions in yeast $tRNA^{Phe}$ as studied with $tRNA^{Phe}$ fragments. *Eur J Biochem* **36:** 76–88.

Romani AM. 2007. Magnesium homeostasis in mammalian cells. *Front Biosci* **12:** 308–331.

Russell R, Millett IS, Tate MW, Kwok LW, Nakatani B, Gruner SM, Mochrie SG, Pande V, Doniach S, Herschlag D, et al. 2002. Rapid compaction during RNA folding. *Proc Natl Acad Sci* **99:** 4266–4271.

Sampson JR, Uhlenbeck OC. 1988. Biochemical and physical characterization of an unmodified yeast phenylalanine transfer RNA transcribed *in vitro*. *Proc Natl Acad Sci* **85:** 1033–1037.

Sattin BD, Zhao W, Travers K, Chu S, Herschlag D. 2008. Direct measurement of tertiary contact cooperativity in RNA folding. *J Am Chem Soc* **130:** 6085–6087.

Sclavi B, Sullivan M, Chance MR, Brenowitz M, Woodson SA. 1998. RNA folding at millisecond intervals by synchrotron hydroxyl radical footprinting. *Science* **279:** 1940–1943.

Serra MJ, Baird JD, Dale T, Fey BL, Retatagos K, Westhof E. 2002. Effects of magnesium ions on the stabilization of RNA oligomers of defined structures. *RNA* **8:** 307–323.

Shiman R, Draper DE. 2000. Stabilization of RNA tertiary structure by monovalent cations. *J Mol Biol* **302:** 79–91.

Siegfried NA, Bevilacqua PC. 2009. Thinking inside the box: Designing, implementing, and interpreting thermodynamic cycles to dissect cooperativity in RNA and DNA folding. *Methods Enzymol* **455:** 365–393.

Sokoloski JE, Dombrowski SE, Bevilacqua PC. 2011. Thermodynamics of ligand binding to a heterogeneous RNA population in the malachite green aptamer. *Biochemistry* **51:** 565–572.

Spink CH, Chaires JB. 1998. Effects of hydration, ion release, and excluded volume on the melting of triplex and duplex DNA. *Biochemistry* **38:** 496–508.

Spink CH, Garbett N, Chaires JB. 2007. Enthalpies of DNA melting in the presence of osmolytes. *Biophys Chem* **126:** 176–185.

Stein A, Crothers DM. 1976a. Conformational changes of transfer RNA. The role of magnesium(II). *Biochemistry* **15:** 160–168.

Stein A, Crothers DM. 1976b. Equilibrium binding of magnesium(II) by *Escherichia coli* $tRNA^{fMet}$. *Biochemistry* **15:** 157–160.

Strulson CA, Molden RC, Keating CD, Bevilacqua PC. 2012. RNA catalysis through compartmentalization. *Nat Chem* **4:** 941–946.

Strulson CA, Yennawar NH, Rambo RP, Bevilacqua PC. 2013. Molecular crowding favors reactivity of a human ribozyme under physiological ionic conditions. *Biochemistry* **52:** 8187–8197.

Swisher JF, Su LJ, Brenowitz M, Anderson VE, Pyle AM. 2002. Productive folding to the native state by a group II intron ribozyme. *J Mol Biol* **315:** 297–310.

Takamoto K, He Q, Morris S, Chance MR, Brenowitz M. 2012. Monovalent cations mediate formation of native tertiary structure of the *Tetrahymena thermophila* ribozyme. *Nat Struct Mol Biol* **9:** 928–933.

Thirumalai D. 1998. Native secondary structure formation in RNA may be a slave to tertiary folding. *Proc Natl Acad Sci* **95:** 11506–11508.

Thirumalai D, Lee N, Woodson SA, Klimov DK. 2001. Early events in RNA folding. *Annu Rev Phys Chem* **52:** 751–762.

Truong DM, Sidote DJ, Russell R, Lambowitz AM. 2013. Enhanced group II intron retrohoming in magnesium-deficient *Escherichia coli* via selection of mutations in the ribozyme core. *Proc Natl Acad Sci* **110:** E3800–E3809.

Turner DH, Bevilacqua PC. 1993. Thermodynamic considerations for evolution by RNA. In *The RNA world* (ed. Gesteland RF, Atkins JF), pp. 447–464. Cold Spring Harbor Laboratory Press, Cold Spring Harbor, NY.

Weikl TR, Palassini M, Dill KA. 2004. Cooperativity in two-state protein folding kinetics. *Protein Sci* **13:** 822–829.

Whitman EE. 2011. "Identification and biophysical characterization of factors influencing the thermostablility of biological RNAs." *Master thesis*, Pennsylvania State University, University Park, PA.

Wilkinson KA, Merino EJ, Weeks KM. 2005. RNA SHAPE chemistry reveals nonhierarchical interactions dominate equilibrium structural transitions in $tRNA^{Asp}$ transcripts. *J Am Chem Soc* **127:** 4659–4667.

Wilkinson KA, Merino EJ, Weeks KM. 2006. Selective 2′-hydroxyl acylation analyzed by primer extension (SHAPE): Quantitative RNA structure analysis at single nucleotide resolution. *Nat Protoc* **1:** 1610–1616.

Wilkinson KA, Gorelick RJ, Vasa SM, Guex N, Rein A, Mathews DH, Giddings MC, Weeks KM. 2008. High-throughput SHAPE analysis reveals structures in HIV-1 genomic RNA strongly conserved across distinct biological states. *PLoS Biol* **6:** e96.

Woodson SA. 2010. Compact intermediates in RNA folding. *Annu Rev Biophys* **39:** 61–77.

Wu M, Tinoco I. 1998. RNA folding causes secondary structure rearrangement. *Proc Natl Acad Sci* **95:** 11555–11560.

Yang SK, Soll DG, Crothers DM. 1972. Properties of a dimer of tRNA I Tyr 1 (*Escherichia coli*). *Biochemistry* **11:** 2311–2320.

Zarrinkar PP, Williamson JR. 1994. Kinetic intermediates in RNA folding. *Science* **265:** 918–924.

Zhou HX, Rivas G, Minton AP. 2008. Macromolecular crowding and confinement: Biochemical, biophysical, and potential physiological consequences. *Annu Rev Biophys* **37:** 375–397.

Zuker M. 2003. Mfold web server for nucleic acid folding and hybridization prediction. *Nucleic Acids Res* **31:** 3406–3415.